Ultrapurification of $SiCl_4$ by Photochlorination in a Bubble Column Reactor

The development and performance of a bubble column photoreactor for ultrapurification of $SiCl_4$ is described. Trichlorosilane ($SiHCl_3$), the principle contaminant in $SiCl_4$ commercially available for use in optical fiber manufacture, is converted to $SiCl_4$ and HCl by UV-initiated photochlorination. Studies of the homogeneous photochlorination kinetics and of Cl_2 gas absorption in a bubble column were undertaken. In addition, an extensive set of data was collected from continuous-flow bubble column reactor (BCR) runs. The rate of photochlorination in the BCR was found to be mass-transfer-limited. A simple model of BCR performance, incorporating the effect of Cl_2 mass transfer rate enhancement by chemical reaction, was tested that agrees well with the experimental data. The BCR was found to be operable over a wide range of $SiHCl_3$ concentrations and $SiCl_4$ feed rates, and capable of lowering the concentration of $SiHCl_3$ in product to below measurable levels (<1 ppm).

David A. Mixon
Michael P. Bohrer
Patricia A. O'Hara
AT&T Bell Laboratories
Murray Hill, NJ 07974

Introduction

Silicon tetrachloride is the primary chemical used in fabrication of optical fiber preforms by the process of Modified Chemical Vapor Deposition (MCVD). Ultrahigh-purity reagents are required to produce low-attenuation lightguides by this technique (MacChesney, 1980; Nagel et al., 1982). Epitaxial-grade $SiCl_4$, a distillate by-product of the manufacture of trichlorosilane ($SiHCl_3$) for the semiconductor industry, is the raw material commercially available in large quantities for MCVD processing. The major contaminant in epitaxial-grade $SiCl_4$ is $SiHCl_3$, which may be present in concentrations up to 10,000 ppm. In the MCVD process $SiCl_4$ vapor is reacted with O_2 at high temperature (>1,800 K) to yield Cl_2 and SiO_2 particles, which are fused to form the lightguiding core of the optical fiber preform. If $SiHCl_3$ is present during this process, IR light-absorbing SiOH will also be formed which leads to IR signal attenuation in the product fiber. Trichlorosilane must therefore be removed from epitaxial-grade $SiCl_4$ in order to maximize the transmission of IR light in optical fibers produced by MCVD.

In response to the recent rapid growth in optical fiber manufacturing, we have developed a relatively simple, yet robust, continuous process for $SiCl_4$ ultrapurification. This process utilizes UV-initiated photochlorination of $SiHCl_3$ in the key purification stage, as has been used in the industry for smaller-scale batch purification (Barns et al., 1980). The continuous process comprises a vertically-sparged, cocurrent-flow bubble-column photoreactor and a packed-bed stripping column arranged in series. The reactor provides for Cl_2 gas absorption and conversion of $SiHCl_3$ to $SiCl_4$ and HCl. The stripping column is used to desorb HCl and excess dissolved Cl_2 from the reactor product by countercurrent contacting with N_2 gas. A heat exchanger downstream of the bubble column regulates the temperature of the stripping column feed. A condenser is located on the gas outlet of the stripping column for recovery of $SiCl_4$ vapor. The HCl, Cl_2, and $SiCl_4$ entrained in the outlet N_2 stream are removed in a gas scrubbing system. Downstream from stripping, the purity of the treated $SiCl_4$ is continuously monitored by in-line IR spectrometry. Product exceeding the impurity limits for $SiHCl_3$ is automatically diverted back to the feed tank.

While design information is readily available for the stripping and heat transfer aspects of continuous $SiCl_4$ purification, little information has been published on either $SiHCl_3$ photochlorination chemistry or absorption of Cl_2 gas in $SiCl_4$, the two processes operative in the bubble column photoreactor. Martynov et al. (1966) have measured the solubility of Cl_2 gas in $SiCl_4$. The patent literature (Takamizawa et al., 1978; Barns et al., 1983) and a related article by Barns et al. (1980) state the feasibility and general requirements for $SiHCl_3$ photochlorination and $SiCl_4$ purification for optical fiber manufacture, without

Correspondence concerning this paper should be addressed to D. A. Mixon.

describing in detail the physical chemical parameters of the reaction. Barns et al. (1980), indicating the liquid-phase reaction is quite rapid, hypothesize a free radical chain reaction involving H abstraction by atomic Cl, formed in solution by the photodissociation of Cl_2 with 330-nm light. Jung et al. (1984) have conducted a study of the kinetics of gas-phase $SiHCl_3$ photochlorination, using the rotating sector technique. In their study, $SiHCl_3$ was used in great excess over Cl_2, and the reaction rate was found to be first order in Cl_2 concentration and half order in absorbed light intensity. A chain mechanism was proposed, with chain termination by coupling of $SiCl_3$ radicals, which yields the experimentally-observed rate expression when solved with the steady-state approximation. The work to date has not produced sufficient data for the engineering design of a heterogeneous reactor with photochlorination in the liquid phase. In this paper we report experimental studies of the homogeneous liquid-phase photochlorination kinetics and of Cl_2 gas mass transfer in a bubble column. We also present the results of an extensive set of pilot-scale bubble column photoreactor runs. A simple reactor model is used to describe the operation of a bubble column photochlorination stage for the continuous $SiCl_4$ ultrapurification process.

Experimental Studies

Materials

Epitaxial-grade $SiCl_4$ was obtained from Dow Corning in a stainless steel 210-L drum, pressurized under a blanket of N_2 (~100 kPa gauge). The drum was equipped with a dip tube and two additional ports to allow venting and pressure transfer of the liquid contents. High-purity-grade (>99.9%) $SiHCl_3$ was obtained from Alfa Chemicals, and high-purity-grade Cl_2 was obtained from Matheson Gas Products. Nitrogen used in contact with the $SiCl_4$ was dried using molecular sieves to prevent $SiCl_4$ hydrolysis.

Chemical analysis

The concentrations of Cl_2 and $SiHCl_3$ in $SiCl_4$ samples were determined by spectrophotometry. Concentrations reported in this work as parts per million (ppm) are based on the weight fraction (wt./wt.). Ultraviolet absorbance measurements of Cl_2 concentration were made in a double-beam instrument (Isco; Model UA-5), with the light-source/absorbance-cell unit located in an exhaust hood. Flow-through absorbance cells, having 0.50-cm light path, were filled by syringe through Teflon tubing and purged with N_2 to empty. Standard Cl_2 solutions were prepared by injecting Cl_2 from a gas-tight syringe into sealed vials containing weighed amounts of $SiCl_4$. For absorption of 326-nm light the Beer-Lambert law was found applicable to Cl_2 solutions limited to concentrations $\leq$500 ppm. The extinction coefficient, ϵ_{Cl}, decreased with increase in Cl_2 concentration above this level. The value of ϵ_{Cl} for Cl_2 concentrations $\leq$500 ppm was determined to be 53.18 L/mol/cm. In measuring Cl_2 concentrations exceeding 500 ppm, sample dilutions were made until successive dilutions showed the linear Beer's law behavior.

The IR absorption band centered at 2,260 cm^{-1} was used to determine $SiHCl_3$. Sample absorbances were measured using a Perkin Elmer Model 683 spectrometer. For the analysis of solutions containing less than 600 ppm $SiHCl_3$, flow-through sample cells with 1.49 and 4.98 cm light paths were fabricated from 1.6-cm (5/8-in.) OD Monel tubing. Silver chloride windows were glued to the tube ends with epoxy. A Perkin Elmer sealed-demountable cell, with silver bromide windows and a light path adjustable from 0.001 to 0.079 cm, was used for the analysis of more concentrated $SiHCl_3$ solutions. The spectral absorbance was found to be linearly proportional to $SiHCl_3$ concentration up to 12,000 ppm, and the Beer's law extinction coefficient, ϵ_{Si}, was measured as 74.19 L/mol/cm.

Apparatus and procedures: photochlorination kinetics

The stoichiometry and the effect of UV light intensity on homogeneous reaction kinetics were studied using a small tubular flow reactor, consisting of a borosilicate glass tube centered within the cylindrical light well of a Rayonet photochemical chamber (Southern New England Ultraviolet Co.; Model RPR-100; fitted with RPR-3500Å UV fluorescent lamps). Solutions of $SiHCl_3$ and Cl_2 in $SiCl_4$ were fed to the reactor from a glass vessel pressurized with N_2. The flow rate was controlled with a metering valve and monitored by rotameter. Reaction samples were taken through a solenoid diverter valve immediately downstream from the reactor. The glass reactor tube had an internal diameter of 4.0 mm and a wall thickness of 1.2 mm. The tube was covered with fiberglass insulation and opaque tape, except for a straight 10.2-mm-long reaction section. A single flow rate of 37.8 mL/min was used, providing a residence time of 0.20 second. The UV lamps used in this system provided radiation centered around 350 nm (black light). The intensity of near-UV light at the position of the reactor tube was varied from 0 to 5,700 $\mu W/cm^2$, as measured with a Blak-ray intensity meter (UltraViolet Products; Model J-221), by adding or removing individual lamps within the light well. The radiation intensity was constant along the length of the reactor tube.

The reaction rate dependence on Cl_2 concentration was studied in batch mode using the analytical UV cell/spectrometer as the photoreactor. Starting solution was injected into the UV cell, and the disappearance of Cl_2 was continuously monitored as a function of batch reaction time, extending up to a maximum of 600 seconds. The 326-nm light source of the spectrometer served both to initiate chlorine radical formation and to measure Cl_2 concentration. The reaction rate dependence on $SiHCl_3$ concentration was also studied in batch mode, by filling an IR cell (1.49-cm light path) with starting solution and exposing it to UV light from a low-pressure mercury lamp for successive 15-second periods up to 150 seconds accumulated reaction time. After each exposure, the cell was placed in the IR spectrometer for $SiHCl_3$ analysis. The transmission of UV light through the cell was found to be stable during the course of a run. In control experiments, with exposure only to ambient room light, the $SiHCl_3$ concentration remained constant for up to 5 minutes.

Apparatus and procedures: chlorine absorption and bubble column performance

Figure 1 shows the design of the experimental bubble column system, which was erected within a large walk-in hood. Materials of construction for contact with $SiCl_4$ were Type 316 stainless steel, borosilicate glass, and Teflon. The important physical

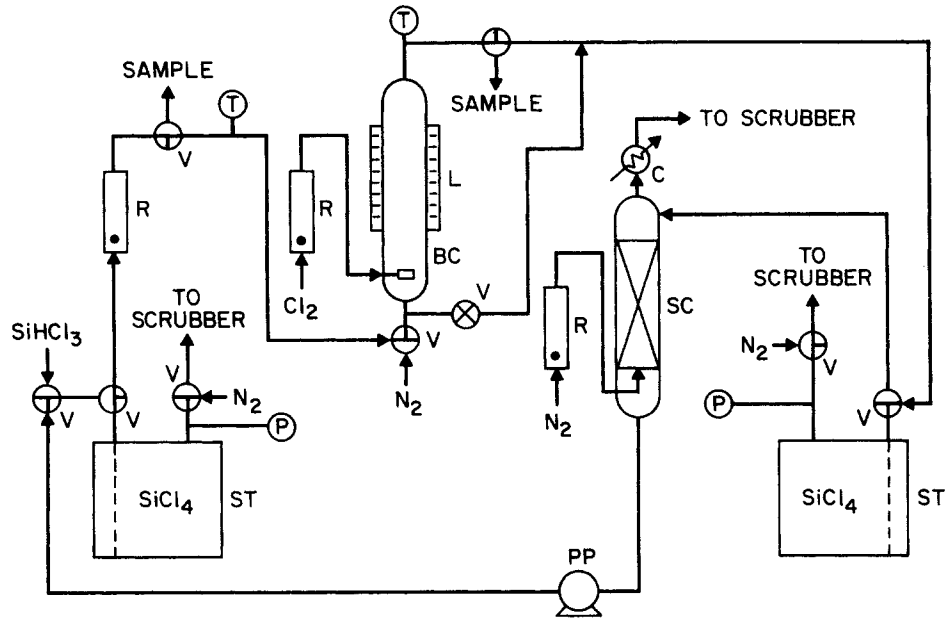

Figure 1. Experimental bubble column reactor system.

design parameters of the bubble column reactor (BCR) and of the two Cl_2 gas spargers tested with it are given in Table 1.

Silicon tetrachloride was fed to the bubble column from a 210-L stainless steel drum, fitted with a dip tube and vapor space ports, by pressurizing the drum with N_2 to ~100 kPa gauge. The $SiCl_4$ feed was doped with $SiHCl_3$ from a small pressure transfer vessel. Homogeneity of the feed was ensured by sparging N_2 through the dip tube to mix the contents. Chlorine was metered into the bubble column through one of two different types of gas sparger (see Table 1). The bubble column effluent was collected in a tank identical to the feed drum. After the $SiCl_4$ feed solution was exhausted, the bubble column effluent was stripped of HCl reaction product and excess Cl_2 using a nitrogen-fed column packed with glass Raschig rings and pumped back to the feed drum for reuse. The flow rates of $SiCl_4$, Cl_2 and N_2 were controlled and monitored using metering valves and rotameters. The BCR feed and reaction temperatures were measured with resistance temperature detector probes.

Table 1. Bubble Column Reactor Design Features

Column ID	0.10 m
Height of UV Reactor Section	1.00 m
Volume of UV Reactor Section	7.85 L
Volume of Gas Sparger Section	1.77 L
Column Wall Thickness	0.006 m
Column Material	Borosilicate glass
Source for UV Illumination	Two banks of dual 30-W UV fluorescent (black light) lamps, mounted 180° apart within an enclosure, spaced ~2 cm from the column wall
Perforated-Plate Sparger	Perforated glass; twelve 0.24-cm-dia. circular holes
Porous Sparger	Sintered glass; 145–175 μm pore size; 12.6 cm^2 sintered glass sparging area

Volumetric mass transfer coefficients for Cl_2 gas absorption in $SiCl_4$ were determined batch-wise in the bubble column, using each of the two gas spargers described in Table 1. For these experiments, the temperature probe shown at the top of the BCR in Figure 1 was replaced with a 0.32-cm (1/8-in.) OD liquid-sampling tube, extending to the center of the BCR for sampling 0.63 m above the gas sparger. Chlorine gas flow rates of 0.74, 1.89 and 2.98 standard L/min were used, corresponding to superficial linear velocities, u_g, of 0.0015, 0.0037 and 0.0058 m/s. At the start of an absorption run, the column was filled with 9.89 L $SiCl_4$, for a liquid height above the sparger of 1.12 m. After taking an initial liquid sample for Cl_2 concentration, Cl_2 gas was sparged for a measured period of time (1 minute for the two higher gas flow rates; 1 to 3 minutes for the lowest gas flow rate). Afterwards, the liquid contents were mixed by sparging N_2 gas into the bottom of the column for 4 seconds, and then sampled for Cl_2 concentration. Increasing the N_2 sparging time from 4 to 10 seconds caused negligible change in the resulting Cl_2 concentration. The measured Cl_2 concentrations were corrected for the dead volume below the gas sparger (0.96 L), so that the C_{Cl} concentrations used to calculate mass transfer coefficients reflect only the absorption volume above the sparger. The sparging/sampling procedure was repeated 10 to 13 times per batch of $SiCl_4$. All runs were carried out at 295 K in duplicate for each sparger design and gas flow rate combination.

Similar experiments were run to determine the fractional Cl_2

gas holdup, ϵ_g, and to obtain an estimate of the bubble size. The measurements taken for calculation of ϵ_g were the heights above the sparger of quiescent liquid and of the gas/liquid mixture during sparging. The corresponding volumes for gas absorption, V_l and V_f, were determined by subtracting the dead volume below the sparger. The height of quiescent liquid was 1.12 m above the sparger for these runs. Bubble size was determined at the midpoint of the bubble column by photography, using a single-lens reflex camera. A 0.64-cm (0.25-in.) OD tube inserted into the bubble column, within the focused photographic range, was used to gauge the bubble size. For nonspherical bubbles, the individual size was taken as the average of the minimum and maximum bubble dimensions. The bubble-size distribution was not determined, and the values reported herein represent the arithmetic mean of those measured.

In studies of reactor performance, the BCR was operated with cocurrent flow of liquid and gas, both entering near the bottom of the column. The disappearance of $SiHCl_3$ was used to gauge reactor performance under steady-state conditions. The existence of steady state was determined by the invariance of reaction temperature and of $SiHCl_3$ and Cl_2 concentrations in consecutive reactor effluent samples and was usually reached 20 to 30 minutes from the start of a run. To begin a run, the empty reactor was filled with $SiCl_4$ which had been doped with the appropriate amount of $SiHCl_3$. The UV lamps were then energized, and the flows of $SiCl_4$ and Cl_2 were initiated and stabilized. After the first steady-state result was measured, up to three additional steady states from the same $SiCl_4$ feed were obtained by altering the UV light intensity or the Cl_2 gas flow rate. The light intensity was varied by energizing none, one or two of the banks of UV lamps housed within the bubble column lamp enclosure. Room temperature air was injected into the annular space between the column and lamp enclosure walls at a rate of ~7.6 m^3/h for cooling. The reactor temperature was monitored with an axial probe, located within the photochlorination section of the bubble column. The temperature of $SiCl_4$ fed to the BCR was ~297 K. Liquid samples were taken from ports located just upstream and downstream of the reactor.

Results and Discussion

Photochlorination kinetics

The chemical kinetic studies were carried out at 296 K. The photochlorination stoichiometry was determined from flow experiments in which both the Cl_2 and $SiHCl_3$ concentrations were measured. The two species were found to react in equimolar amounts, within experimental uncertainty (mole ratio = 1.01 ± 0.11) so that the overall liquid-phase reaction may be adequately described by,

$$SiHCl_3 + Cl_2 \xrightarrow{h\nu} SiCl_4 + HCl \qquad (1)$$

The dimer Si_2Cl_6, which could be formed by combination of $SiCl_3$ radicals (Jung et al., 1984), was not observed in the IR spectra from any of the photochlorination reaction mixtures.

The results of batch kinetic runs were analyzed using the following rate expression:

$$\text{rate} = -\frac{dC_{Cl}}{dt} = -\frac{dC_{Si}}{dt} = kC_{Si}^{\alpha}C_{Cl}^{\beta} \qquad (2)$$

where C_{Cl} and C_{Si} are the molar concentrations of Cl_2 and $SiHCl_3$ in $SiCl_4$. The method of excess was used to determine the exponents α and β. Time-concentration data were taken for one reactant, while maintaining the concentration of the other reactant essentially constant by using it in ~25-fold molar excess. The starting concentration of the species to be measured was kept in the range of 300 to 500 ppm. For example, in the determination of β, Eq. 2 reduces to

$$-\frac{dC_{Cl}}{dt} = (kC_{Si}^{\alpha})C_{Cl}^{\beta} = k^*C_{Cl}^{\beta} \qquad (3)$$

The experimental data were compared to the integrated forms of Eq. 3 for half-integral values of β ranging from ½ to 2. The exponent was determined from the best data fit (least squares linear regression) to the integrated rate equations. The values of α and β were found to be ½ and 1, respectively, yielding the expression,

$$\text{rate} = kC_{Si}^{1/2}C_{Cl} \qquad (4)$$

Figures 2 and 3 show typical time-concentration experimental data for $SiHCl_3$ and Cl_2, along with the data fit using Eq. 4.

Assuming 1:1 reaction stoichiometry ($C_{Cl,i} - C_{Cl} = C_{Si,i} - C_{Si}$), Eq. 4 may be integrated to yield the following:

$$kt = \frac{2}{\sqrt{C_{Cl,i} - C_{Si,i}}}\left[\tan^{-1}\left(-\frac{\sqrt{C_{Si}}}{\sqrt{C_{Cl,i} - C_{Si,i}}}\right)\right]_i^f \qquad (5)$$

for $C_{Cl,i} > C_{Si,i}$, and

$$kt = \frac{1}{\sqrt{C_{Si,i} - C_{Cl,i}}}\left[\ln\left(\frac{-\sqrt{C_{Si}} - \sqrt{C_{Si,i} - C_{Cl,i}}}{-\sqrt{C_{Si}} + \sqrt{C_{Si,i} - C_{Cl,i}}}\right)\right]_i^f \qquad (6)$$

for $C_{Cl,i} < C_{Si,i}$,

where t is the residence time, and i and f denote initial and final conditions. These equations were used to evaluate k, from flow reaction data, for UV light intensities incident upon the reactor

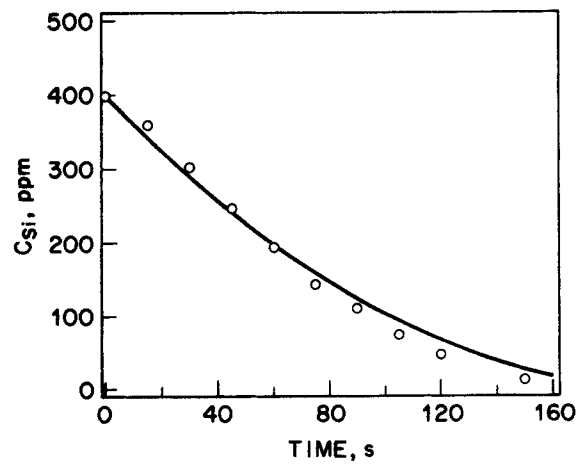

Figure 2. Time-concentration data for $SiHCl_3$ photochlorination in excess Cl_2.
Experimental points and data fit for α = ½ (solid line)

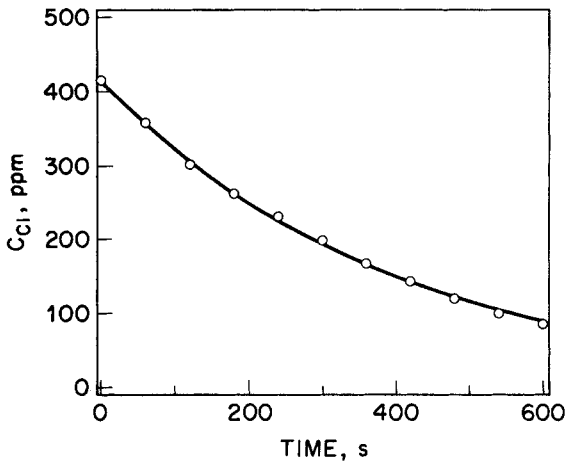

Figure 3. Time-concentration data for $SiHCl_3$ photochlorination in excess $SiHCl_3$.
Experimental points and data fit for $\beta = 1$ (solid line)

tube wall, I_w, ranging from 0 to 5,700 $\mu W/cm^2$. In these experiments, the uncertainties in measured Cl_2 and $SiHCl_3$ concentrations were $\sim \pm 10\%$ and $\pm 5\%$, respectively, leading to a maximum uncertainty in the calculated k values of $\sim \pm 50\%$. The value of k was found to be linearly proportional to $I_w^{1/2}$, as shown in Figure 4. The slope of the solid line (data fit) in Figure 4 yields a value of 1.17 $(L/mol)^{1/2}/(\mu W/cm^2)^{1/2}/s$ for k', in the expression,

$$\text{rate} = k' I_w^{1/2} C_{Si}^{1/2} C_{Cl} \tag{7}$$

No reaction was observed in the total absence of UV irradiation. In these light intensity experiments, the concentration of Cl_2 in the reactor feed was less than 500 ppm. Both the absorption of incident light and the Cl_2 concentration change in the 4-mm ID reactor tube were small. In this case, the overall measured reaction rate may be equated to the radially-dependent local rates averaged over the reactor diameter solely with respect to light intensity. Using the diffuse light irradiation model of Matsuura and Smith (1970) for the approximation of no light attenuation, the radially-averaged light intensity over the cross section of the reactor, $\bar{I}_r$, is related to I_w as

$$\bar{I}_r = 2 I_w \tag{8}$$

In addition, under these experimental conditions the radially-averaged absorbed light intensity, $\bar{I}_a$, and $\bar{I}_r$ are related as

$$\bar{I}_a = \epsilon_{Cl} C_{Cl} \bar{I}_r \tag{9}$$

Then, the reaction rate equation may be written as follows:

$$\begin{aligned} \text{rate} &= k'(2\epsilon_{Cl} C_{Cl})^{-1/2} \bar{I}_a^{1/2} C_{Si}^{1/2} C_{Cl} \\ &= k^0 \bar{I}_a^{1/2} C_{Si}^{1/2} C_{Cl}^{1/2} \end{aligned} \tag{10}$$

with k^o having a value of 0.113 $(cm^3/\mu W)/s$. The Cl_2 concentration is restricted to 500 ppm or less for this equation to be valid.

The relationship in Eq. 10 is consistent with a free radical chain reaction mechanism initiated by light absorption and terminated by bimolecular coupling of the active chain carriers (Calvert and Pitts, 1966). According to this analysis, the true reaction order with respect to Cl_2 is ½, and the apparent Cl_2 reaction order of 1 given in Eqs. 4 and 7 is due to the dependence of $\bar{I}_a$ on C_{Cl} in Eq. 9, which holds for Cl_2 concentrations ≤ 500 ppm according to Beer's law. This result is in contradiction to the findings of Jung et al., who report an overall gas-phase photochlorination rate that is proportional to the product $(I_a^{1/2} \cdot C_{Cl})$, when the $SiHCl_3$ pressure is much greater than the Cl_2 pressure. To our knowledge, the reaction orders for Cl_2 and $SiHCl_3$ given in Eq. 10 cannot be derived from a simple mechanism based on a single termination step. The absence of Si_2Cl_6 reaction product and the existence of 1:1 Cl_2:$SiHCl_3$ photochlorination stoichiometry indicate that termination involving two $SiCl_3$ radicals is probably not occurring, as claimed in the gas-phase reaction mechanism proposed by Jung et al.

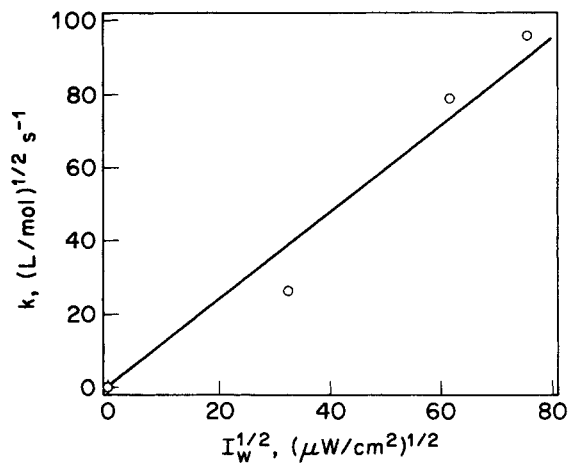

Figure 4. Chemical kinetic parameter, k vs. $I_w^{1/2}$.

Chlorine gas absorption

The Cl_2 gas absorption data were analyzed using the following relationship for mass transfer:

$$\frac{dC_{Cl}}{dt} = \frac{K_g a [P_{Cl} - (C_{Cl}/C_T) H]}{(1 - \epsilon_g)} \tag{11}$$

where

K_g = overall mass transfer coefficient based on the pressure driving force
a = specific interfacial area
P_{Cl} = partial pressure of Cl_2 in the gas phase
C_T = total liquid-phase concentration of all species
H = thermodynamic Henry's law coefficient for Cl_2 gas solubility in $SiCl_4$

The value of H(kPa) can be obtained from the relation,

$$H = 101.3 \times 10^{(-924/T + 3.93)} \tag{12}$$

where T is the absolute temperature (Martynov et al., 1966). At 101.3 kPa (1 atm) and 298 K, the maximum solubility of Cl_2 in $SiCl_4$ is 0.148 mol fraction, or 67,600 ppm. For the 1:1 photochlorination stoichiometry 5,240 ppm Cl_2 is needed to react with 10,000 ppm $SiHCl_3$. Mass transfer was studied for Cl_2 concen-

trations up to 4,790 ppm, and the measured mass transport rates were found to be independent of Cl_2 concentration in this range.

Under the assumptions that column operation is isothermal and that the specific molar volume of a dilute $Cl_2/SiCl_4$ solution is equal to that of pure $SiCl_4$, Eq. 11 may be integrated and solved for the volumetric mass transfer coefficient, $K_g a$:

$$K_g a = \frac{(1-\epsilon_g)}{t} \cdot \left[\frac{C_{Cl}}{(P_{Cl}-H)} - \frac{C^o H}{(P_{Cl}-H)^2} \cdot \ln\{C^o P_{Cl} + C_{Cl}(P_{Cl}-H)\}\right]_i^f \quad (13)$$

where t is the run duration and C^o is the molar density of pure $SiCl_4$. The value of ϵ_g was found from experimental data by the relationship, $\epsilon_g = (V_f - V_l)/V_f$. The partial pressure of Cl_2 gas was taken as 109.4 kPa, the arithmetic mean of pressures at the top and bottom of the liquid column. The value for C^o at 295 K is 8.71 mol/L.

The mass transfer experiments were carried out nominally within the "quiescent bubbling" flow regime, which is encountered for superficial gas velocities $u_g < 0.05$ m/s in many systems where the liquid-phase viscosity is water-like. This regime is normally characterized by the presence of uniformly-sized bubbles having equal radial distribution. Although homogeneous bubble distribution was not rigorously verified, homogeneity was visually apparent for $u_g \geq 0.0037$ m/s using the porous sparger, and for $u_g = 0.0058$ m/s using the perforated-plate sparger. For smaller u_g, the bubble distribution was obviously nonhomogeneous, with bubbles tending to rise in a column separated from the walls. Bubble size using the porous sparger (0.5 to 2 mm) was smaller than that using the perforated plate sparger (3 to 7 mm) for each gas velocity tested.

Table 2 summarizes the results of the mass transfer experiments. The overall mass transfer coefficient K_g is related to the individual coefficients by the following:

$$\frac{1}{K_g} = \frac{1}{k_g} + \frac{H'}{k_l} \quad (14)$$

where k_g and k_l are the individual mass transfer coefficients based on gas-side and liquid-side bulk/interfacial concentration differences, and H' is the Henry's law coefficient in units of kPa · $(L/\text{mol})(\approx H/C^o)$. Mass transfer resistance in the gas phase is negligible due to the use of pure Cl_2 gas, thereby reducing Eq. 14 to,

$$k_l = H' K_g \quad (15)$$

Table 2. Mass Transfer Experimental Results

f_g	u_g ($\times 10^2$)	Gas Sparger Design	$K_g a$ ($\times 10^6$)	$k_l a$ ($\times 10^4$)	ϵ_g ($\times 10^2$)
0.74	0.15	Perforated plate	0.33	0.24	0.18
1.89	0.37		0.79	0.58	0.36
2.98	0.59		1.38	1.01	0.51
0.74	0.15	Porous	0.50	0.37	0.32
1.89	0.37		1.27	0.93	0.47
2.98	0.59		2.03	1.48	0.61

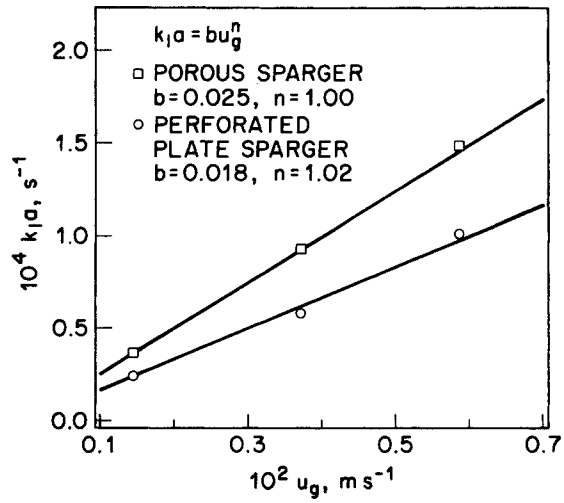

Figure 5. Plot of Eq. 16, $k_l a$ vs. u_g for porous and perforated plate spargers.
With experimental data included

and enabling calculation of $k_l a$. The data for $k_l a$ were fit to a correlation of the type,

$$k_l a = b u_g^n \quad (16)$$

after Deckwer et al. (1974), where b and n are empirical constants. Figure 5 presents the experimental data and plots of Eq. 16 for both spargers. The value of $k_l a$ depends strongly on both gas superficial velocity and sparger design. The rate of physical absorption of Cl_2 gas increases with u_g and is higher for the porous sparger than for the perforated plate sparger. The net Cl_2 gas absorption for each gas flow rate is ~95% using the porous sparger and ~62% using the perforated plate sparger.

The data for ϵ_g were also fit to an equation of the form,

$$\epsilon_g = b' u_g^{n'} \quad (17)$$

where b' and n' are constants (after Shah et al., 1982). Figure 6

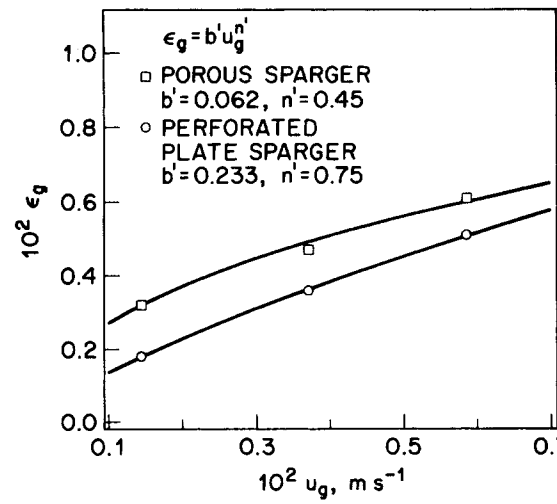

Figure 6. Plot of Eq. 17, ϵ_g vs. u_g, for porous and perforated plate spargers.
With experimental data included

presents these data and plots of Eq. 17 for both spargers. Although the values of ϵ_g are very small due to both the high rate of Cl_2 absorption and the low superficial gas velocities used, they are also dependent on sparger type and u_g.

Bubble column reactor performance

Continuous-flow photochlorination experiments were carried out using the BCR either with the perforated-plate sparger or the porous sparger. Table 3 lists the reaction conditions and results of 14 runs, including the increase in temperature, the concentrations of $SiHCl_3$ and Cl_2 in the feed and product, the volumetric feed rates of $SiCl_4$ and Cl_2 gas, and the molar feed ratio of Cl_2: $SiHCl_3$. The flow rate of effluent Cl_2 gas was calculated from a mass balance on the measured Cl_2 and $SiHCl_3$ flows, accounting for the disappearance of Cl_2 by reaction according to Eq. 1. In these runs, the Cl_2 gas outflow was found to vary from 5 to -9 mmol/min, values of which are indistinguishable from zero within the accuracy of the calculation. For a Cl_2:$SiHCl_3$ molar feed ratio ≤ 1, all the Cl_2 gas fed is consumed by reaction. For a molar ratio >1, the excess Cl_2 gas is completely absorbed into solution. Only in run 15-a, where there is no direct UV illumination, is Cl_2 detected in appreciable amounts in reactor effluent containing $SiHCl_3$. This indicates that, in the presence of chemical reaction and for the UV light

Table 3. Reaction Conditions and Results for Continuous-Flow BCR Photochlorination Experiments

	Feed Rate (L/min)**		Feed Conc. (ppm)		Feed Ratio (molar)	Product Conc. (ppm)		
Exp. No.*	$SiCl_4$	Cl_2(g)	$SiHCl_3$	Cl_2(Soln)	Cl_2:$SiHCl_3$	$SiHCl_3$	Cl_2(Soln)	ΔT_R(K)
2-a(4)		2.75			0.92	1,122	0	19
2-b(4)	1.03	2.98	11,248	98	0.99	310	8	21
2-c(4)		3.45			1.15	0	610	22
2-d(4)		3.14			1.04	0	142	21
3-a(2)		2.98			1.05	0	345	20
3-b(2)	1.03	2.60	10,505	34	0.91	559	5	18
3-c(4)		2.60			0.91	422	0	18
3-d(4)		2.78			0.98	0	106	20
4-a(2)		3.98			0.92	617	19	19
4-b(4)	1.55	3.98	10,607	33	0.92	539	19	19
4-c(4)		4.22			0.98	161	17	21
5-a(4)	1.55	4.46	11,714	18	0.93	580	21	23
5-b(4)		4.79			1.00	0	281	24
6-a(2)		1.51			0.91	593	20	11
6-b(4)	1.03	1.51	6,134	26	0.91	424	24	12
6-c(4)		1.69			1.02	0	27	13
7-a(4)		1.89			0.95	445	33	14
7-b(4)	1.03	2.10	7,422	49	1.06	0	246	15
7-c(4)		2.52			1.26	0	1,111	15
8-a(4)	1.03	0.24	980	25	0.96	84	0	3
8-b(4)		0.27			1.06	0	26	3
9-a(4)	1.03	0.10	380	49	1.26	0	63	2
9-b(4)		0.12			1.37	15	65	2
10-a(4)		0.08			1.12	100	66	2
10-b(4)	1.03	0.13	382	64	1.54	0	83	2
10-c(4)		0.16			1.88	0	145	2
11-a(4)		0.08			1.07	137	43	2
11-b(4)	1.03	0.12	399	67	1.38	0	77	2
11-c(4)		0.14			1.60	0	116	2
12-a(4)		0.29			1.03	17	8	3
12-b(4)	1.03	0.33	1,109	42	1.16	0	100	3
12-c(4)		0.37			1.30	0	210	4
13-a(4)		1.51			0.89	570	19	12
13-b(4)	1.03	1.69	6,292	39	1.00	0	0	13
13-c(4)		1.83			1.09	0	250	13
14-a(4)		2.03			0.82	1,423	0	15
14-b(4)	1.03	2.38	9,110	21	0.96	254	0	18
14-c(4)		2.75			1.12	0	399	18
15-a(0)		0.71			0.99	2,285	1,510	0
15-b(2)	1.03	0.71	2,822	116	0.99	64	82	6
15-c(4)		0.71			0.99	103	86	6

*Runs 2-10 employ the perforated plate sparger; runs 11-15 employ the porous sparger; the number in parentheses indicates the number of UV lamps used.
**The gas feed rate is given at 101 kPa, 295 K.

intensities used, the overall rate of $SiHCl_3$ conversion is controlled by the absorption rate of Cl_2 gas.

The experimental results for mass transfer without chemical reaction indicate a higher Cl_2 gas absorption rate with the porous sparger than with the perforated-plate sparger. However, a comparison of runs with approximately equal starting concentrations of $SiHCl_3$ (runs 6 vs. 13; 8 vs. 12; 10 vs. 11) shows that there is virtually no difference in BCR performance using either of the two types of sparger. This may be explained by the combined action of two phenomena modifying Cl_2 gas absorption occurring simultaneously with $SiHCl_3$ photochlorination. First, the $SiCl_4$ used is saturated with N_2 as a result of shipping and storage under a N_2 gas blanket (~100 kPa gauge). During reaction, extensive nitrogen bubble formation occurs throughout the liquid, resulting from desorption due to depressurization (column pressure is ~5 kPa gauge) and temperature rise. The *in situ* evolution of nitrogen bubbles perturbs the Cl_2 gas bubble swarm and mixes the reaction mixture, tending to equalize the results obtained with either sparger. Second, mass transfer may be enhanced when accompanied by a fast chemical reaction. In addition to increasing the intrinsic mass transfer rate, the chemical reaction effectively reduces the bulk liquid-phase Cl_2 concentration, providing a larger concentration-gradient driving force for absorption (Astarita et al., 1983).

Runs 3, 4, 6 and 15 demonstrate the effect of UV light intensity on the BCR photochlorination rate. Reduction of incident UV intensity from 3,080 $\mu W/cm^2$ (four UV lamps) to 1,540 $\mu W/cm^2$ (two UV lamps) has very little effect on the concentration of $SiHCl_3$ in the reactor product. The largest difference occurs in run 6, where reduction of the UV intensity results in a product $SiHCl_3$ concentration 169 ppm higher. The extreme sensitivity of this system to very low levels of UV irradiation may be seen in run 15, where 19% conversion of $SiHCl_3$ is reached without use of the UV lamps. Stray room light is responsible for this result, since thermal or dark reactions were found to be negligible. Unlike the small reactor used for the kinetic studies, it was impossible to completely shield the BCR from room light.

The performance limit of the BCR has not been exceeded in these runs. Under the most demanding conditions used (run 5), with a $SiCl_4$ flow rate of 1.55 L/min and $SiHCl_3$ feed concentration of 11,714 ppm, a Cl_2:$SiHCl_3$ molar feed ratio of 1.001 is sufficient to reduce the product $SiHCl_3$ concentration to below measurable levels. The Cl_2 gas flow rate used in this run is 4.79 standard L/min. The BCR performance is just as efficient at the lowest liquid (1.03 L/min) and gas flow rates (0.08–0.16 standard L/min) used, as indicated by the results of runs 9, 10 and 11. Our findings indicate that the molar feed ratio of Cl_2:$SiHCl_3$ is the key variable for conversion of $SiHCl_3$ in this size reactor and for these flow rates. In most cases, a flow of Cl_2 gas slightly in excess of stoichiometric results in complete conversion of $SiHCl_3$.

A simple model of steady-state BCR performance was formulated from the material and energy balance for an ideal mixed reactor. In this analysis, the column is broken up into two sections: the sparger section below the UV lamps, where only mass transfer occurs; and the reactor section which is directly exposed to UV light.

The set of equations used to model the reactor section follows:

$$(C_{Si,i} - C_{Si})Q = V_R(1 - \epsilon_g)k^o\epsilon_{Cl}^{1/2}\bar{I}_r^{1/2}C_{Si}^{1/2}C_{Cl} \quad (18)$$

$$(C_{Cl} - C_{Cl,i})Q = K_g a V_R\left(P_{Cl} - \frac{C_{Cl}}{C^o}H\right) - V_R(1 - \epsilon_g)k^o\epsilon_{Cl}^{1/2}\bar{I}_r^{1/2}C_{Si}^{1/2}C_{Cl} \quad (19)$$

$$(T - T_i)\rho c_p Q = -\Delta H_R V_R(1 - \epsilon_g)k^o\epsilon_{Cl}^{1/2}\bar{I}_r^{1/2}C_{Si}^{1/2}C_{Cl} - U_{id}A_{id}\Delta T_L \quad (20)$$

where

i = inlet to the reactor section
Q = volumetric flow rate of $SiCl_4$
V_R = reactor section volume
ρ = $SiCl_4$ mass density
c_p = $SiCl_4$ heat capacity
ΔH_R = enthalpy of reaction
U_{id}, A_{id} = overall heat transfer coefficient and area based on the inside column diameter
ΔT_L = log mean temperature driving force for heat transfer from the column

The values of $K_g a$ and ϵ_g are obtained from the Cl_2 gas superficial velocity at column pressure and temperature, according to Eqs. 15, 16 and 17. The concentration of dissolved Cl_2 entering the reactor section is found from the rate of physical absorption of Cl_2 gas in the sparger section:

$$C_{Cl,i}Q = K_g a V_S\left(P_{Cl} - \frac{C_{Cl,i}}{C^o}H\right) \quad (21)$$

where V_S is the sparger section volume.

The model assumes perfect mixing in the liquid phase, negligible resistance to gas-phase mass transfer, and negligible vapor pressure for $SiHCl_3$ and $SiCl_4$. The chemical reaction rate term, $k^o\epsilon_{Cl}^{1/2}\bar{I}_r^{1/2}C_{Si}^{1/2}C_{Cl}$, is obtained from Eqs. 9 and 10. Therefore, the model pertains only to conditions under which the dissolved Cl_2 concentration in the reactor is ≤500 ppm. The value of $\bar{I}_r^{1/2}$ is calculated as a function of I_w, C_{Cl}, and reactor diameter, using the diffuse light irradiation model as described by Matsuura and Smith (1970). In this way, the reaction rate term is explicitly dependent upon these variables. Due to the lack of precise information on the bubble-size distribution and velocities and due to the lack of a suitable theoretical model (Alfano et al., 1986), the influence of bubble-induced light scattering on the absorbed intensity has not been incorporated in the BCR model calculations. In addition, the model does not account for the appreciable gas shrinkage expected from the high rate of Cl_2 absorption. Nor does it directly account for any of the effects of N_2 gas desorption during reaction. However, N_2 outgassing significantly increases the level of agitation in the reactor, strengthening the assumption of perfect mixing. Nitrogen outgassing reduces the validity for application of the axial dispersion mixing model, which is normally applied to bubble-column performance in the quiescent bubbling flow regime (Deckwer et al., 1974; Szeri et al., 1976).

Table 4 lists the numerical values of parameters used for solution of the model equations. The value of H varies with temperature according to Eq. 12. The $SiCl_4$ mass density ρ and molar density C^o depend upon temperature as shown in Table 4 (Washburn et al., 1928). The mass transfer coefficient $K_g a$ is assigned a temperature proportionality of $T^{2/3}$. The lack of an

Table 4. Numerical Values of BCR Model Parameters

I_w (4 UV lamps)	3,080 μW/cm^2
I_w (2 UV lamps)	1,540 μW/cm^2
V_R	7.85 L
V_S	1.77 L
k^o	0.113 (cm^3/μW)$^{1/2}$/s
ϵ_{Cl}	53.18 L/mol/cm
ρ	$1.524-(1.975 \times 10^{-3})T - (7.14 \times 10^{-7})T^2 - (4.9 \times 10^{-8})T^3$ (where T is in °C), kg/L
c_p	842 J/kg/K
ΔH_R	254.1 kJ/mol
U_{id}	9.8 J/m^2/K/s

activation energy for the chemical reaction rate is not expected to significantly alter the outcome of the model, due to the observed mass transfer control of the BCR photochlorination rate for the UV light intensities used. The heat transfer coefficient U_{id} is calculated from the cooling gas heat capacity, flow rate, and inlet/outlet temperatures, and from the reactor temperature measured for the BCR runs. The heat of reaction is calculated from heat of formation data (Karapet'yants, 1970). The heat capacity of $SiCl_4$ is taken from a Dow Corning publication (Dow Corning, 1981). Heat input, due to radiation from the UV lamps, is negligible, as evidenced by the experimental finding of an immeasurable temperature rise under flow conditions with no reaction.

The model, Eqs. 18 through 20, was solved numerically. Representative results are shown, in comparison with experiment, in Table 5 and in Figures 7 and 8. In Table 5, the experimental reactor volume is compared with the reactor volume predicted for selected BCR runs, using both the porous and perforated-plate spargers. While the actual value of V_R is 7.85 L, the predicted V_R ranges from 12.19 to 13.77 L for the perforated plate and from 8.24 to 8.85 L for the porous sparger. If the BCR model is modified by the inclusion of a mass transfer enhancement factor, E_f, the predicted and experimental reactor volumes may be reconciled. The values of E_f required for this are given in Table 5. The average E_f is 1.64 for the perforated-plate sparger

Table 5. Model Predictions for BCR Volume

Experimental BCR Volume = 7.85 L			
Exp. No.	Sparger Design	Predicted BCR Vol. (L)*	Mass Transfer Enhancement Factor**
2-a	Perforated	12.33	1.56
2-b		12.19	1.54
3-c		13.30	1.68
4-b		12.85	1.63
4-c		12.47	1.58
5-b		12.87	1.63
6-b		13.60	1.72
7-a		12.94	1.64
8-a		13.77	1.75
12-a	Porous	8.70	1.11
13-a		8.78	1.14
14-a		8.85	1.13
14-b		8.56	1.09
14-c		8.24	1.05
15-c		8.61	1.10

*Using K_La determined in the absence of chemical reaction (see Figure 5).
**Multiplier of mass transfer term in Eq. 19, required to bring experimental and predicted BCR volumes into agreement.

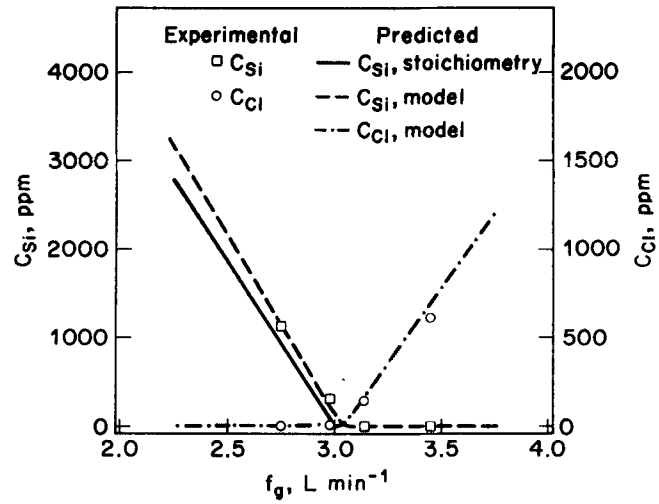

Figure 7. Model plot of $SiHCl_3$ and Cl_2 concentrations in reactor product vs. feed Cl_2 gas flow for perforated plate sparger.
Reaction conditions and experimental data from Run 2; solid line indicates the results expected if all the Cl_2 gas fed is consumed by reaction

and 1.10 for the porous sparger, leading to average predicted reactor volumes of 7.84 (σ = 0.35) and 7.87 (σ = 0.22), respectively. The use of these average mass transfer enhancement factors in the model brings the predicted and experimental reactor volumes into reasonably good agreement over the entire range of reaction conditions used in this study.

Figures 7 and 8 show the predicted and observed concentrations of Cl_2 and $SiHCl_3$ in the BCR product as a function of Cl_2 gas feed rate, f_g, for runs 2 and 14 using the perforated-plate and porous spargers, respectively. The values of E_f from Table 5 were used in the model calculations. Both the model and experimental data demonstrate that the Cl_2 concentration in the reactor is negligible when the molar feed rate of $SiHCl_3$ exceeds that

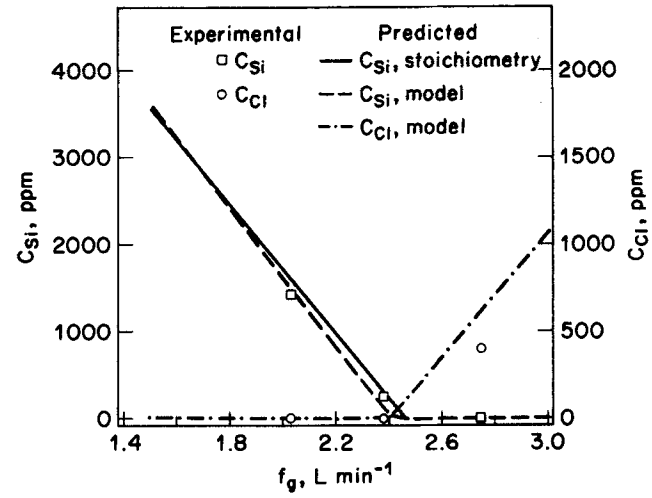

Figure 8. Model plot of $SiHCl_3$ and Cl_2 concentrations in reactor product vs. feed Cl_2 gas flow for porous sparger.
Reaction conditions and experimental data from Run 14; solid line indicates the results expected if all the Cl_2 gas fed is consumed by reaction

of Cl_2, and for I_w between 1,540 and 3,080 $\mu W/cm^2$. For Cl_2:$SiHCl_3$ molar feed ratios >1, the product Cl_2 concentration is elevated and the $SiHCl_3$ concentration is effectively zero. Moreover, the differences in results among those predicted by the stoichiometric ratio of reactant feeds, model predictions, and experimental values are all within the limits of accumulated experimental error. It is apparent from these figures that the Cl_2 gas fed to the BCR is completely reacted and that the use of both sparger types produces this result. Enhancement of mass transfer by chemical reaction is the overriding factor in reactor performance for this system.

The influence of radiation intensity in the model is examined by calculating the required reactor volume for the conditions of run 14-a using different values for I_w. As expected, increasing I_w has no influence on the model predictions. Reducing I_w by a factor of 2 also produces no change in the model prediction. In order to cause the predicted reactor volume to increase by 5%, the value of I_w must be reduced by a factor of $>2 \times 10^4$, equivalent to a ~160-fold reduction in the reaction rate. Thus, the conversion of $SiHCl_3$ may remain mass-transfer-controlled even when the reaction rate is reduced by more than two orders of magnitude.

Conclusions

In this work we have proposed and studied a novel and industrially important application of bubble column reactor technology. The UV-induced photochlorination of $SiHCl_3$ in a BCR has been shown to be very effective in reducing the level of this contaminant in epitaxial-grade $SiCl_4$ to sub-ppm concentrations. The mass transport and chemical kinetics involved in this system have been studied, both separately and together using a pilot-scale continuous-flow bubble column photoreactor.

The physical mass transfer rate for Cl_2 gas absorption in $SiCl_4$ was found to depend on both sparger design and Cl_2 superficial gas velocity. A porous sparger generates smaller bubbles and provides higher mass transfer rates than a perforated-plate sparger, for superficial gas velocities ranging from 0.0015 to 0.0058 m/s. The net Cl_2 gas absorption was found to be ~95% for the porous sparger and ~62% for the perforated-plate sparger. However, when the BCR is used for $SiHCl_3$ photochlorination, the mass transfer rate is evidently enhanced by chemical reaction. This is inferred from the observation that under UV irradiation conditions, for both sparger types and the entire range of u_g studied, 100% of the Cl_2 gas fed is reacted with $SiHCl_3$ present in the BCR. Therefore, the sparger type and u_g, while affecting the physical mass transfer rates, do not significantly affect BCR performance.

The liquid-phase homogeneous photochlorination kinetics and stoichiometry were determined at 296 K. A 1:1 stoichiometry was observed for the UV-induced reaction of Cl_2 and $SiHCl_3$. The dimer Si_2Cl_6 was not produced under any of the reaction conditions used. The experimentally determined rate expression is given by Eq. 10, which shows half-order dependence on $SiHCl_3$ and Cl_2 concentrations. The rate of photochlorination was found to be proportional to the square root of the average absorbed light intensity, indicating a free radical reaction mechanism with bimolecular termination of chain-carrying species.

In an extensive set of continuous-flow BCR runs, Cl_2 was not observed to coexist in solution with $SiHCl_3$ under UV irradiation conditions, indicating overall mass transfer control in the two-phase reactor. For $SiCl_4$ flow rates ranging from 1.03 to 1.55 L/min and $SiHCl_3$ concentrations from 400 to 12,000 ppm, the $SiHCl_3$ is completely converted to $SiCl_4$ with a very slight stoichiometric excess of Cl_2 gas fed. The BCR performance is insensitive to variations of incident UV radiation intensity in the range between 1,540 and 3,080 $\mu W/cm^2$. A simple ideal mixed-flow model, incorporating the effect of mass transfer enhancement by chemical reaction, was found to be adequately descriptive of reactor performance over the range of reaction conditions studied.

Notation

a = specific interfacial area, dm^2/L of gas-liquid dispersion
A_{id} = area for heat transfer in a bubble column based on inside diameter, m^2
b, b' = empirical constants in Eqs. 16 and 17
c_p = heat capacity of $SiCl_4$, J/kg/K
C^o = molar density of $SiCl_4$, mol/L
C_{Cl} = final or outlet concentration of Cl_2, mol/L (or ppm)
$C_{Cl,i}$ = initial or inlet concentration of Cl_2, mol/L
C_{Si} = final or outlet concentration of $SiHCl_3$, mol/L (or ppm)
$C_{Si,i}$ = initial or inlet concentration of $SiHCl_3$, mol/L
C_T = total concentration of all species, mol/L
E_f = mass transfer enhancement factor, dimensionless
f_g = Cl_2 volumetric gas flow rate, L/min (101 kPa, 295 K)
H = Henry's law coefficient for Cl_2 in $SiCl_4$, kPa
H' = Henry's law coefficient for Cl_2 in $SiCl_4$, $\approx(H/C^o)$, kPa · L/mol
I_w = incident light intensity at reactor wall, $\mu W/cm^2$
I_r = radially averaged incident light intensity, $\mu W/cm^2$
I_a = average absorbed light intensity, $\mu W/cm^3$
k = photochlorination rate constant, $(L/mol)^{1/2}/s$
k' = photochlorination rate constant, $(L/mol)^{1/2}/(\mu W/cm^2)^{1/2}/s$
k^o = photochlorination rate constant, $(cm^3/\mu W)^{1/2}/s$
k^* = pseudorate constant defined in Eq. 3
k_g = gas-phase mass transfer coefficient, $mol/dm^2/kPa/s$
k_l = liquid-phase mass transfer coefficient, dm/s
K_g = overall mass transfer coefficient based on pressure driving force, $mol/dm^2/kPa/s$
n, n' = empirical constants in Eqs. 16 and 17
P_{Cl} = partial pressure of Cl_2, kPa
Q = volumetric flow rate, L/s
t = time, s
T = temperature, K
T_i = temperature at the reactor section inlet, K
u_g = Cl_2 superficial gas velocity, m/s
U_{id} = overall heat transfer coefficient in a bubble column based on inside diameter, $J/m^2/K/s$
V_f = volume of gas/liquid mixture above gas sparger, L
V_l = volume of quiescent liquid above gas sparger, L
V_R = volume of reactor section of bubble column, L
V_S = volume of sparger section of bubble column, L

Greek letters

α = exponent in kinetic Eqs. 2 and 3
β = exponent in kinetic Eqs. 2 and 3
ΔH_R = enthalpy of photochlorination reaction, J/mol
ΔT_L = log mean temperature driving force for heat transfer in a bubble column, K
ΔT_R = temperature increase in BCR due to reaction, K
ϵ_g = fractional gas holdup
ϵ_{Cl} = Beer's law extinction coefficient for Cl_2 in $SiCl_4$ at 326 nm, L/mol/cm
ϵ_{Si} = Beer's law extinction coefficient for $SiHCl_3$ in $SiCl_4$ at 2,260 cm^{-1}, L/mol/cm
ρ = mass density of $SiCl_4$, kg/L

Literature Cited

Astarita, G., D. W. Savage, and A. Bisio, *Gas Treating with Chemical Solvents*, Wiley, New York (1983).
Alfano, O. M., R. L. Romero, and A. E. Cassano, "Radiation Field

Modelling in Photoreactors-II. Heterogeneous Media," *Chem. Eng. Sci.*, **41**, 1137 (1986).

Barns, R. L., E. A. Chandross, D. L. Flamm, L. T. Manzione, and L. F. Thompson, "Purification Process for Compounds Useful in Optical Fiber Manufacture," U.S. Patent No. 4372834 A (1983).

Barns, R. L., E. A. Chandross, and C. M. Melliar-Smith, "The Photochemical Purification of the Reagents Used in the MCVD Optical Fiber Process," Eur. Conf. of Optical Commun., IEEE Conf. Publ. No. 190, 26 (1980).

Calvert, J. G., and J. N. Pitts, Jr., *Photochemistry*, Wiley, New York (1966).

Deckwer, W.-D., R. Burckhart, and G. Zoll, "Mixing and Mass Transfer in Tall Bubble Columns," *Chem. Eng. Sci.*, **29**, 2177 (1974).

Dow Corning, *Properties and Essential Information for Handling and Use of Chlorosilanes*, Midland, MI (1981).

Jung, K.-H., J. S. Shin, and Y. S. Choi, "Photochlorination Reaction of Trichlorosilane ($SiHCl_3$) at 337.1 nm," *Bull. of Korean Chem. Soc.*, **5**(6), 260 (1984).

Karapet'yants, M. Kh., and M. L. Karapet'yants, *Thermodynamic Constants of Inorganic and Organic Compounds*, Ann Arbor-Humphrey Science Publ. (1970).

MacChesney, J. B., "Materials and Processes for Preform Fabrication-Modified Chemical Vapor Deposition and Plasma Chemical Vapor Deposition," *Proc. of the IEEE*, **68**(10), 1181 (1980).

Martynov, Y. M., I. B. Davidovskaya-Chemelinskaya, and E. K. Borodulina, "Solubility of Chlorine in Tetrachlorides," *Zhurnal Prikladnoi Khimii*, USSR, **39**(12), 2650 (1966).

Matsuura, T., and J. M. Smith, "Light Distribution in Cylindrical Photoreactors," *AIChE J.*, **16**(2), 321 (1970).

Nagel, S. R., J. B. MacChesney, and K. L. Walker, "An Overview of the Modified Chemical Vapor Deposition (MCVD) Process and Performance," *IEEE J. of Quantum Electronics*, **QE-18**(4), 459 (1982).

Shah, Y. T., B. G. Kelkar, S. P. Godbole, and W.-D. Deckwer, "Design Parameters Estimations for Bubble Column Reactors," *AIChE J.*, **28**(3), 353 (1982).

Szeri, A., Y. T. Shah, and A. Madgavkar, "Axial Dispersion in Two Phase Co-current Flow with Fast and Instantaneous Reactions," *Chem. Eng. Sci.*, **31**, 225 (1976).

Takamizawa, M., H. Okamoto, M. Unemura, and K. Koya, "Purification of Silicon Tetrachloride," *Ger. Offen.* DE 2805824 (1978).

Washburn, E. W., C. J. West, N. E. Dorsey, F. R. Bichowsky, and A. Klemenc, eds., *International Critical Tables*, McGraw-Hill, New York (1928).

Manuscript received Jan. 18, 1989, and revision received Nov. 28, 1989.